BULLETIN OF THE POLISH ACADEMY OF SCIENCES
TECHNICAL SCIENCES, Vol. 69(5), 2021, Article number: e137586
DOI: 10.24425/bpasts.2021.137586

Synthesis of Mg-based alloys with rare-earth element addition by means of mechanical alloying

Sabina LESZ[1*], Bartłomiej HRAPKOWICZ[1], Klaudiusz GOŁOMBEK[1], Małgorzata KAROLUS[2], and Patrycja JANIAK[1]

[1] Department of Engineering Materials and Biomaterials, Silesian University of Technology, ul. Konarskiego 18A, 44-100, Gliwice, Poland
[2] Institute of Materials Engineering, University of Silesia, ul. 75 Pułku Piechoty 1a, 41-500 Chorzów, Poland

Abstract. Magnesium-based alloys are widely used in the construction, automotive, aviation and medical industries. There are many parameters that can be modified during their synthesis in order to obtain an alloy with the desired microstructure and advantageous properties. Modifications to the chemical composition and parameters of the synthesis process are of key importance. In this work, an Mg-based alloy with a rare-earth element addition was synthesized by means of mechanical alloying (MA). The aim of this work was to study the effect of milling times on the Mg-based alloy with a rare-earth addition on its structure and microhardness. A powder mixture of pure elements was milled in a SPEX 8000D high energy shaker ball mill under an argon atmosphere using a stainless steel container and balls. The sample was mechanically alloyed at the following milling times: 3, 5, 8 and 13 h, with 0.5 h interruptions. The microstructure and hardness of samples were investigated. The Mg-based powder alloy was examined by means of X-ray diffraction (XRD), scanning electron microscopy (SEM) and using a Vickers microhardness test. The results showed that microhardness of the sample milled for 13 h was higher than that of those with milling time of 3, 5 and 8 h.

Key words: mechanical alloying; magnesium; rare-earth element; ytterbium.

1. INTRODUCTION

Nowadays, medicine is characterized by dynamic development – yesterday's innovations in treatment will be outdated by tomorrow. Due to the increasing emphasis placed on the improvement of patients' comfort and life quality, modern implantology is facing far greater challenges than ever before. Thus in the wake of growing expectations, material science has to rise to the occasion and constantly deliver advanced materials, with unique properties and unusual applications [1–11]. From that point of view, particularly interesting are those biomaterials which are as highly non-intrusive for the human body homeostasis as possible. The ideal biomaterial model, initially assuming total corrosion resistance, has evolved under the influence of increasing popularity of biodegradable materials [12, 13]. Hence, there is a growing demand for materials whose properties include decomposition lacking a toxic effect not only on the internal environment of living organisms, but more importantly, presence of a beneficial therapeutic impact on the surrounding tissues [2, 3].

Among well-known bioinert conventionally used metallic materials, including stainless steels, Co-Cr and Ti based alloys [4], materials composed of elements already existing in the human body, have attracted considerable attention [5, 6]. According to Staiger *et al*. [7], magnesium, in addition to being an indispensable cofactor of key enzymes for metabolism as well as a natural component of bones, remains completely non-toxic to the body and is innoxiously excreted in the urine. Magnesium and its lightweight alloys are particularly interesting in biomedical applications owing to their abovementioned good biodegradability and promising mechanical and physical properties [8, 14]. Elastic modulus, compressive yield strength and density are comparable to that of natural bone, thereby reducing the risk of osteopenia and avoiding osteolysis [1, 5, 15]. However, the fundamental issue in applying crystalline magnesium-based implants is their poor corrosion resistance as compared to the fast formation of hydrogen cavities around the implant [16–19]. Therefore, this may imply potential difficulties in healing of the damaged tissues and, as a consequence, the necessity of reoperation in order to remove the faulty implant [20]. Moreover, due to the nature of a crystal structure, solid solutions always have limited solubility of the solute, which makes it difficult to add other elements to improve the alloy. It thus becomes necessary to apply novel processing techniques and parameters which make it possible to obtain an amorphous structure. Amorphous bulk metallic glasses are well-known for their homogeneous atomic structure, which allows for dissolution of many elements, even in large concentrations [8, 21]. Therefore Löffler *et al*. [22] have proven that addition of zinc as an alloying element, above the threshold of 28% contribution, significantly increases corrosion resistance and reduces activity of hydrogen cavities formations.

As claimed by Byrne *et al*. [23], amorphous magnesium-based alloys presented a decreasing corrosion rate which directly

*e-mail: sabina.lesz@polsl.pl

Manuscript submitted 2021-02-26, revised 2021-05-08, initially accepted for publication 2021-05-10, published in October 2021

affects reduced hydrogen evolution, permeation and a lower tendency to form hydrogen cavities. It is reported that the improved corrosion resistance is justified by the absence of defects in the amorphous structure, e.g. grain boundaries [15, 24]. Corrosion resistance can also be improved by Ca addition to Mg alloys [25]. For example, the AZ91Ca alloy exhibited a five-fold increase in surface film resistance as compared with the AZ91 alloy [26]. Wang *et al*. [27] demonstrated that the biodegradation rate of an AZ31 alloy can be significantly reduced as a result of grain refinement produced by mechanical processing. Guangyin *et al*. [28] declared that addition of calcium to Mg-based alloys efficiently reduces grain size, hence its presence in the alloy is beneficial.

There are several techniques in which bulk metallic glasses can be produced, but undoubtedly mechanical alloying has attracted significant attention in recent reports [8, 29, 30]. It is a solid state powder preparation method, based on repeated flattering, cold-welding, fracturing and rewelding of powder particles during a dry or wet high-energy milling process, often in special atmospheres. Interaction occurs by way of collisions between the powdered particles, the ball and the container wall. Thus homogenization takes place. As a result, extremely finely ground powder (grain size below 1 μm) is obtained [31, 32]. However there is a major disadvantage of this method in the context of magnesium-based alloys, since the alloys obtained are characterized by significant brittleness. Previous studies indicate that alloying with addition of rare-earth elements to improve mechanical properties can be a promising method [29, 33, 34]. Ytterbium as a rare-earth element is fully biocompatible and well-known to increase the glass-forming ability. It is used to thermally stabilize the alloy [24]. Research conducted by Yu *et al*. [21] confirmed that adding ytterbium to magnesium-based alloys significantly enhanced their ductility. Moreover, Liang *et al*. [29] reported that compressive strength of Mg-Zn-Ca alloys increased following the addition of ytterbium. Recent scientific reports suggest that ytterbium dopants in the bone structures are exhibited as a novel strategy in bone defect treatment [35].

2. MATERIALS AND METHODS

2.1. Materials

For the fabrication of the sample, high purity elements (>99.5%) of Mg, Zn, Ca and Yb were mechanically alloyed in a dual high-energy ball mill (SPEX 8000D). Element composition of the powders is shown in Table 1. A hardened steel vial and balls were the milling media, and the ball-to-powder weight ratio was 10:1 [3, 8, 36]. We conducted mechanical alloying (MA) in an argon atmosphere, for different durations of 3, 5, 8 and 13 h.

Table 1
Element composition of the Mg-Zn-Ca-Yb powders

Element	Mg	Zn	Ca	Yb
at.%	62.00	33.00	4.00	1.00
wt.%	37.69	53.97	4.01	4.33

2.2. Methods

The constituent phases of the mechanically alloyed powders were examined by the X-ray diffraction (XRD) technique (PANalytical Empyrean Diffractometer, X-ray Cu radiation $\lambda_{K\alpha} = 1.5418$ Å). The lattice strain, lattice parameter and crystallite size from the spectra were estimated by using the Rietveld refinement integrated with the High Score Plus PANalytical software [37]. Phase analysis was performed with ICDD PDF4+ data base.

The powder morphology in a scanning electron microscope (SEM, Zeiss SUPRA 35) was studied. The energy-dispersive spectrometer EDS (Trident XM4 EDS with 20 kV of accelerating voltage) analysis was carried out on the samples after 3, 5, 8 and 13 h of milling time. Particle size analysis using ImageJ Software was also conducted. Chemical analysis was performed on the metallurgical specimen. The metallurgical specimen were ground and polished following standard procedure. Accuracy of the main and major element in wt.% are 2% and 4%, respectively, and for minor and trace elements are in a range of 10–20% and 50–100%, respectively.

For the determination of particle size distribution (PSD) of powders, a laser particle size measuring instrument (Fritsch Analysette 22 MicroTec+) was used. The sample powders are added to a closed circuit filled with an appropriate liquid. Therefore, wet dispersion analysis was used. In this case samples were measured in ethyl alcohol as a dispersant. The characteristic median diameter (d_{50}) was determined.

Microhardness tests were carried out on polished samples using a Vickers hardness tester (Future-Tech FM700) with a load of 50 grams of force applied for 15 seconds. At least 5 measurements under the same conditions were conducted for each sample, and the average value was used as their microhardness (HV).

3. RESULTS AND DISCUSSION

The XRD patterns of the Mg-Zn-Ca-Yb powders, mechanically alloyed for different milling times: 3, 5, 8 and 13 h, are presented in Fig. 1. The XRD patterns revealed the presence of a phase having a hexagonal close-packed (HCP) crystal structure Mg (solid state solution) and $MgZn_2$, traces of Ca_5Zn_3 and $CaMg_2$ phases and the presence of unreacted Zn and Yb precursors. The $MgZn_2$ phases characteristic peaks are shown after the milling process due to the mechanical alloying processes between Mg and Zn. The original sharp diffraction lines of Mg gradually become broader and their intensity decreases with milling time. After 13 hours of milling, one can observe relaxation of the main phases structure and increasing of their crystallite size. The structural analysis results obtained for the materials studied is presented in Table 2.

Figure 2 compares the scanning electron microscopy (SEM) images of the powders mechanically alloyed at different milling times: 3, 5, 8 and 13 h.

The shapes and morphology of the powders are similar to one another and were irregular owing to repeated cold-welding and fracturing during MA [3, 8, 36]. The average particle size was ~57, 51 and 36 μm, after milling time of 3, 5 and 8 h,

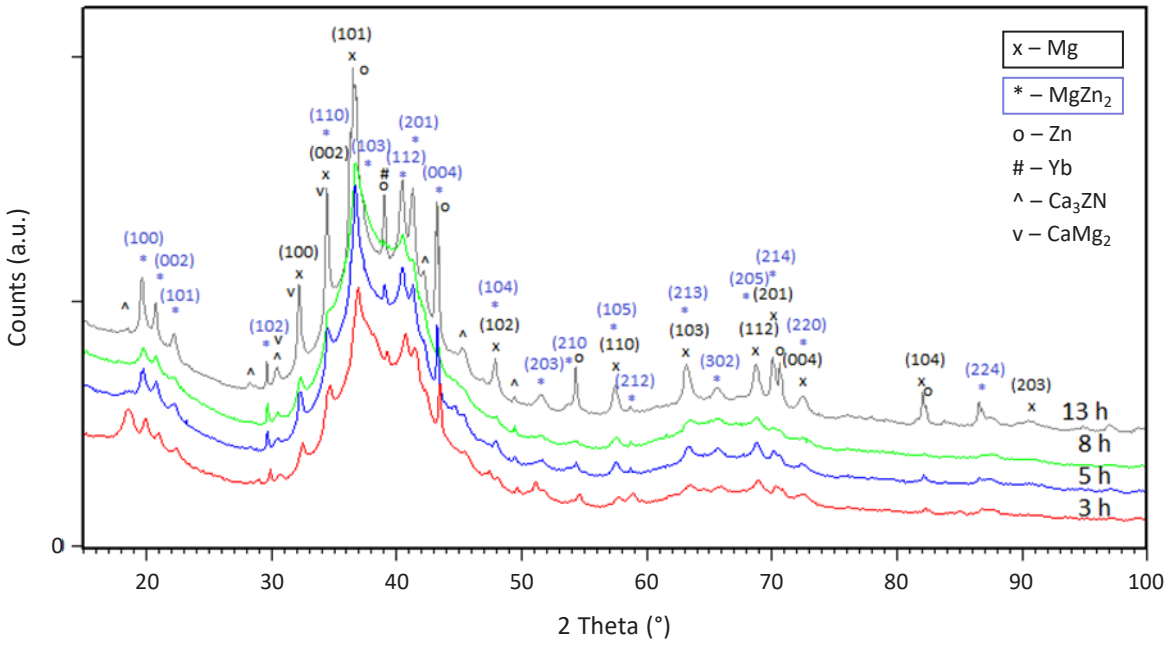

Fig. 1. X-ray diffraction patterns of the Mg-Zn-Ca-Yb powders milled for 3, 5, 8 and 13 h

Table 2

Crystallite size and changes of unit cell parameters of the main phases preset in alloys after different milling times: solid state solution based on hexagonal Mg and intermetallic $MgZn_2$ phase

Sample (milling time)	Mg(Zn,Yb,Ca)				$MgZn_2$			
	Theoretical (ICDD PDF4+ card: 04–015–0486)	Refined (RR) a/c [Å]	Crystallite size D [Å]	Lattice strain η [%]	Theoretical (ICDD PDF4+ card: 04–008–7744)	Refined (RR) a/c [Å]	Crystallite size D [Å]	Lattice strain η [%]
3	a = 3.2110 c = 5.2130 Space group: $P6_3/mmc$ Crystallographic system: hexagonal	3.2012(4) 5.1131(3)	400	1.17	a = 5.2210 c = 8.5670 Space group: $P6_3/mmc$ Crystallographic system: hexagonal	5.4026(9) 8.3412(5)	300	0.37
5		3.2022(2) 5.1311(8)	350	1.17		5.2949(9) 8.7643(1)	270	0.37
8		3.1941(7) 5.0964(3)	290	0.37		5.3466(7) 8.6679(1)	210	0.06
13		3.2019(2) 5.2009(7)	370	0.43		5.3015(9) 8.8776(4)	320	0.05

respectively. The results of SEM analysis for the samples milled for 13h (Fig. 2d) reveal that homogeneous powders are formed with fine particle sizes of about 18 μm.

The XRD (Fig. 1) and SEM (Fig. 2) analysis revealed that Mg-Zn-Ca-Yb powders mechanically alloyed in an argon atmosphere were micron-sized powders constituting a nanocrystalline Mg-based solid state solution and $MgZn_2$ phases.

Figure 3 shows a measured example of the cumulative curve for samples milled for 3, 5, 8 and 13 h. The diameters (d_{10}, d_{50}, d_{90}) determined the various characteristic fractions of powders within PSD and are presented in Table 3. All of the results were presented as the mean ± standard deviation (SD).

Table 3

Characteristic diameters (d_{10}, d_{50}, d_{90}) of various fractions of powders. Results for samples milled for 3, 5, 8 and 13 h and accuracy

Sample	Characteristic diameters (μm)		
	d_{10}	d_{50}	d_{90}
3 h	13 ± 1.1	66 ± 4.5	163 ± 22.1
5 h	11 ± 1.3	56 ± 5.5	106 ± 7.6
8 h	12 ± 0.9	43 ± 5.1	103 ± 11.5
13 h	6.5 ± 0.1	20 ± 0.5	41 ± 1.9

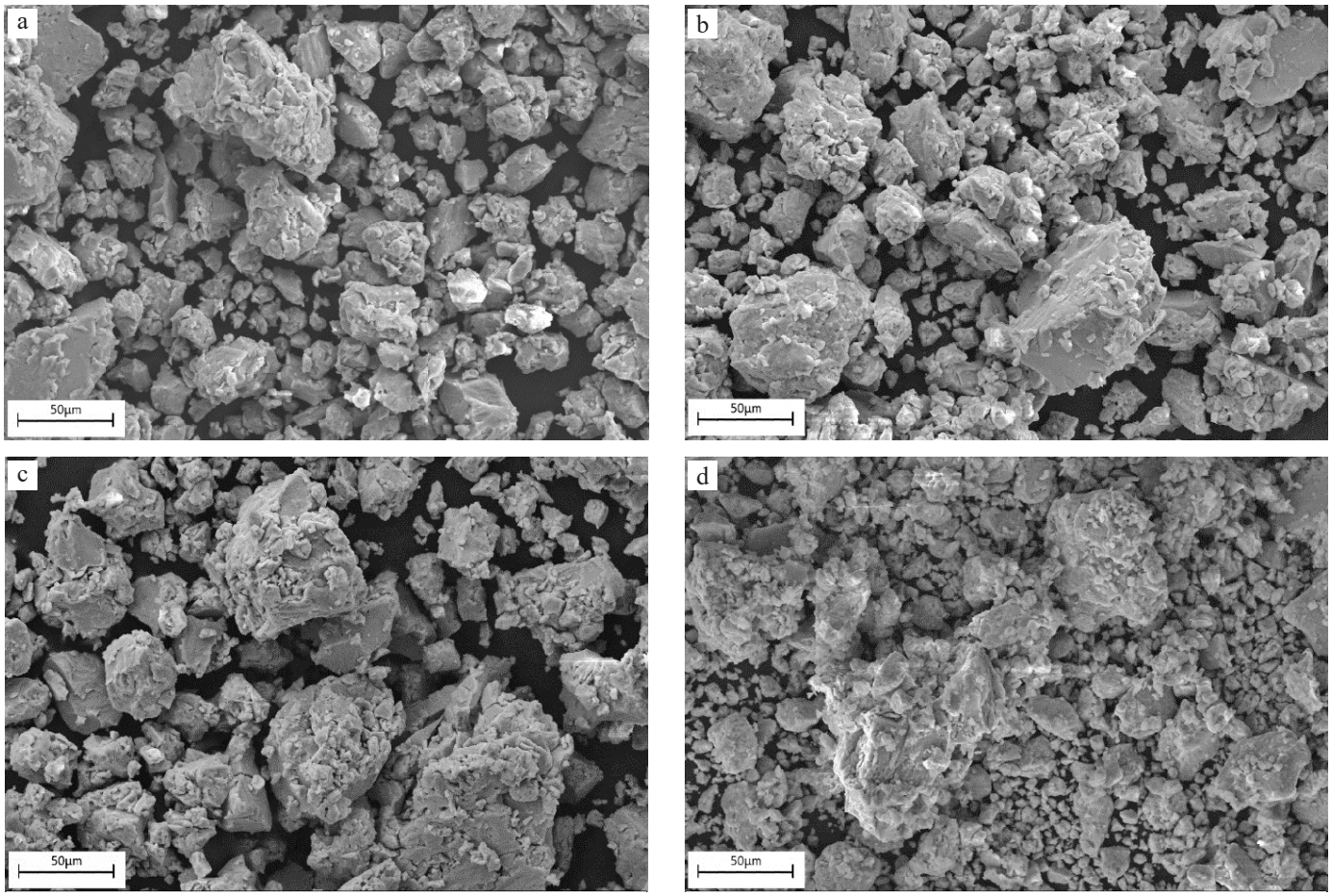

Fig. 2. SEM images of Mg-Zn-Ca-Yb powders milled for 3 (a), 5 (b), 8 (c) and 13 h (d)

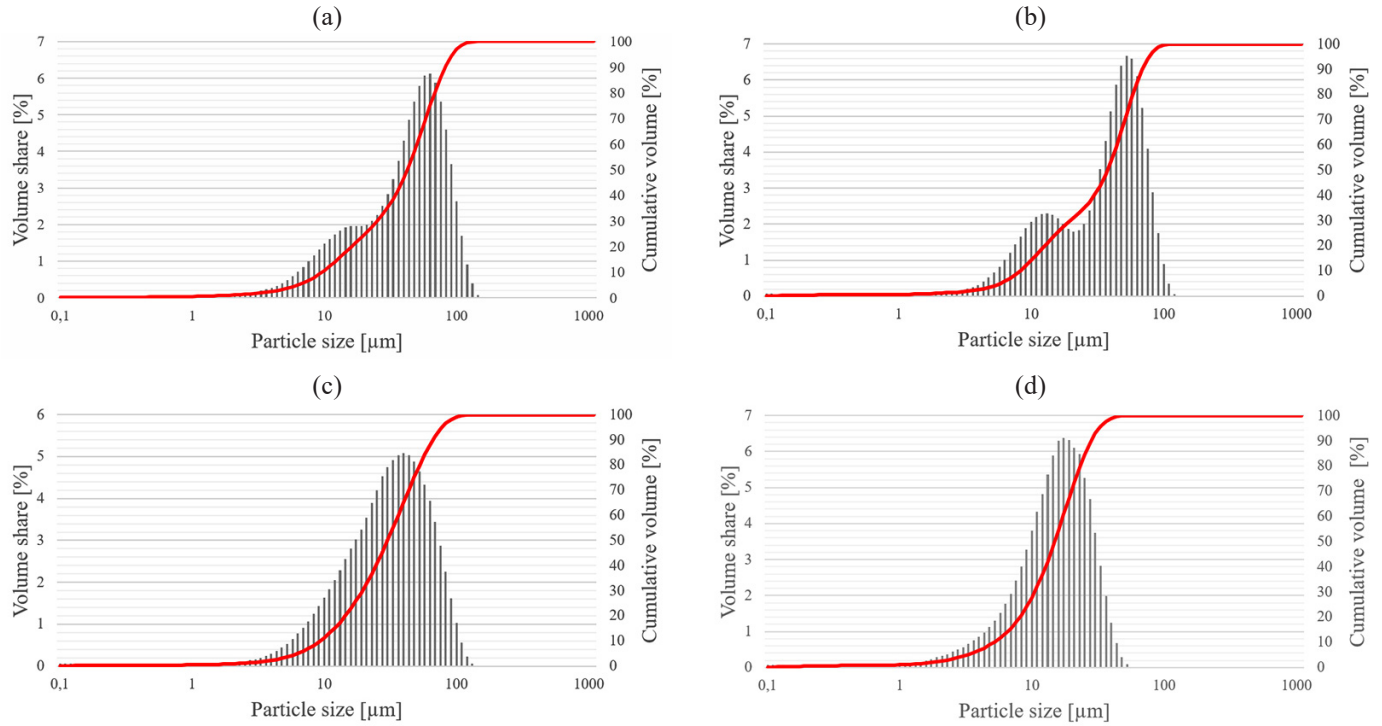

Fig. 3. Cumulative curve for Mg-Zn-Ca-Yb samples milled for 3 (a), 5 (b), 8 (c) and 13 h (d)

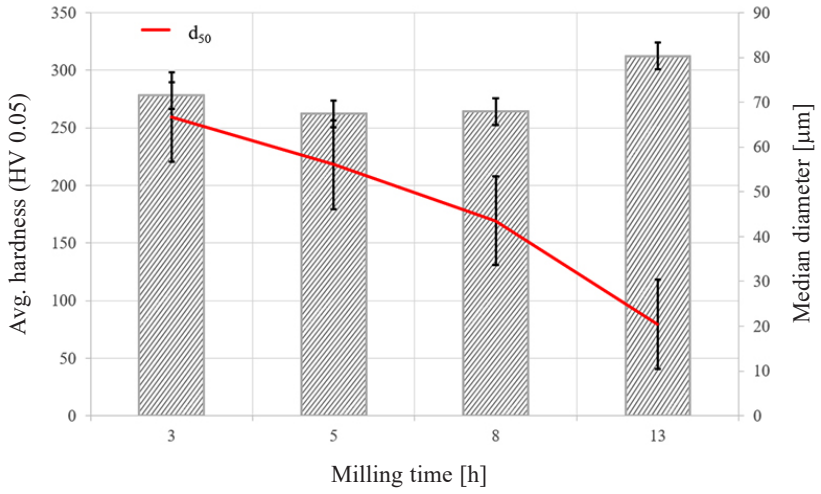

Fig. 4. Effect of milling time on microhardness (HV) and median diameter (d_{50}) determined for each powder

In the initial stage of the mechanical alloying (MA) process, PSD (particle size distribution) is characterized by two peaks (Fig. 3a, 3b) and this is explained by the fact that the investigated powders are a mixture of particles with a largely differentiated size. This fact might be related to the presence of two different main phases: Mg-based solid state solution and $MgZn_2$. Extending the milling time to 8 hours resulted in the distribution curve. It is characterized as an asymmetric deviation (Fig. 3c) in the next stage of MA. A high fraction of large particles is formed as a result of multiple welding (Fig. 3c). The asymmetry is far less distinct and this is related to the cracking of large particles described earlier. In the last stage, a symmetric, relatively narrow distribution curve implies that the process has reached the set condition, showing the state of balance between the mechanisms of joining and fragmentation (Fig. 3d).

Each hardness value was the average of five measurements for every sample, as shown in Table 4. In Fig. 4 the influence of milling time on median diameters (d_{50}) of particles and the average microhardness value was presented. Figure 4 shows the average microhardness value and median diameter (d_{50}) for all samples.

Based on the diagram (Fig. 4, Table 4), the highest value of microhardness was found in the sample that had been milled for 13 h (312 ± 15 HV). Meanwhile, the lowest value was obtained from a sample milled for 5 h (262 ± 32 HV). The sample milled for 8 h had a similar value of microhardness (264 ± 28). The sample milled for 3 h had the value of microhardness of 278 ± 48 HV.

Table 4

Hardness value with accuracy for samples milled for 3, 5, 8 and 13 h

Test number	Microhardness (HV 0.05) of samples milled for			
	3 h	5 h	8 h	13 h
1	210	244	263	305
2	316	221	246	290
3	309	261	242	322
4	326	319	306	336
5	229	266	306	309
Average:	**278 ± 48**	**262 ± 32**	**264 ± 28**	**312 ± 15**

In the first stage of the MA process, wide hardness dispersion occurs (Table 4, Fig. 4). The particle sizes are both smaller and larger (Fig. 3a) because some of the powder particles are trapped between the grinding balls and show strong deformation while others remain intact [8, 38, 39]. The saturation of hardness (Table 4, Fig. 4) after 13 h of milling time is related to the narrow dispersion of particle sizes occurring in the last stage of MA (Fig. 3d).

The chemical compositions of these samples tested by EDS are given in Table 5. The measured chemical compositions are

Table 5

Chemical composition of the samples. EDS (energy-dispersive spectroscopy) results for samples milled for 3, 5, 8 and 13 h, respectively. Accuracy of the main elements is about 4 wt.% and minor and trace elements are in the range of 20–50 wt.%

Sample (milling time)	at.%					wt.%				
	Mg	Zn	Ca	Yb	O	Mg	Zn	Ca	Yb	O
3	61.7	29.2	4.4	1.2	3.5	39.3	50.0	4.6	4.5	1.6
5	61.4	28.7	5.6	1.1	3.2	39.0	48.9	5.9	4.9	1.3
8	62.9	29.7	3.5	1.2	2.7	39.7	50.3	3.6	5.2	1.2
13	61.9	25.4	7.4	1.8	3.5	40.0	44.6	7.8	5.9	1.7

slightly different from nominal ones, which is likely due to the oxidation of Mg during preparation of the sample for the SEM study.

4. CONCLUSIONS

The aim of this work is the synthesis of Mg-based alloys with addition of a rare-earth element (ytterbium) by means of mechanical alloying, performed in order to study the effect of milling times on the structure, morphology and microhardness.

The XRD diffraction pattern analysis showed that the milling process (gradually for 3, 5 and 8 hours) leads to the formation of two main nanocrystalline phases: an α-Mg solid state solution and intermetallic $MgZn_2$ phase. The crystallite sizes of both phases are in the range of 200–400 Å.

The compositional homogeneity of the alloys remained consistent with the intended chemical composition.

The alloy milled for 13 hours of milling time provided the highest value of microhardness, which stood at 312 HV. The saturation of hardness is related to the narrow dispersion of particle sizes ($d_{10} = 6.5$, $d_{90} = 41$ μm) occurring in the last stage of MA. The particle sizes of the powders decreased with increased milling time. The values of the median diameter (d_{50}) were calculated as 66, 56, 43 and 20 μm for Mg-Zn-Ca-Yb after 3, 5, 8 and 13 h of milling time, respectively.

ACKNOWLEDGEMENTS

This research was funded by the National Science Centre, Poland, grant number 2017/27/B/ST8/02927.

REFERENCES

[1] F. Witte, "The history of biodegradable magnesium implants: A review," *Acta Biomater.*, vol. 6, no. 5, pp. 1680–1692, 2010.

[2] N. Eliaz, "Corrosion of metallic biomaterials: A review," *Materials (Basel).*, vol. 12, no. 3, 2019.

[3] S. Lesz, J. Kraczla, and R. Nowosielski, "Structure and compression strength characteristics of the sintered Mg-Zn-Ca-Gd alloy for medical applications," *Arch. Civ. Mech. Eng.*, vol. 18, no. 4, pp. 1288–1299, 2018.

[4] T. Narushima, *New-generation metallic biomaterials*, 2nd ed. Elsevier Ltd., 2019.

[5] D. Persaud-Sharma and A. Mcgoron, "Biodegradable magnesium alloys: A review of material development and applications," *J. Biomim. Biomater. Tissue Eng.*, vol. 12, no. 1, pp. 25–39, 2012.

[6] N. Sezer, Z. Evis, S.M. Kayhan, A. Tahmasebifar, and M. Koç, "Review of magnesium-based biomaterials and their applications," *J. Magnes. Alloy.*, vol. 6, no. 1, pp. 23–43, 2018.

[7] M.P. Staiger, A.M. Pietak, J. Huadmai, and G. Dias, "Magnesium and its alloys as orthopedic biomaterials: A review," *Biomaterials*, vol. 27, no. 9, pp. 1728–1734, Mar. 2006.

[8] S. Lesz, B. Hrapkowicz, M. Karolus, and K. Gołombek, "Characteristics of the Mg-Zn-Ca-Gd alloy after mechanical alloying," *Materials (Basel).*, vol. 14, no. 1, pp. 1–14, 2021.

[9] A. Drygała, L.A. Dobrzański, M. Szindler, M. Prokopiuk Vel Prokopowicz, M. Pawlyta, and K. Lukaszkowicz, "Carbon nanotubes counter electrode for dye-sensitized solar cells application," *Arch. Metall. Mater.*, vol. 61, no. 2A, pp. 803–806, 2016.

[10] A. Drygała, M. Szindler, M. Szindler, and E. Jonda, "Atomic layer deposition of TiO_2 blocking layers for dye-sensitized solar cells," *Microelectron. Int.*, vol. 37, no. 2, pp. 87–93, 2020.

[11] M. Beniyel, M. Sivapragash, S.C. Vettivel, and P.S. Kumar, "Optimization of tribology parameters of AZ91D magnesium alloy in dry sliding condition using response surface methodology and genetic algorithm," *Bull. Polish Acad. Sci. Tech. Sci.*, pp. 1–10, 2021.

[12] L.A. Dobrzański, L.B. Dobrzański, and A.D. Dobrzańska-Danikiewicz, "Manufacturing technologies thick-layer coatings on various substrates and manufacturing gradient materials using powders of metals, their alloys and ceramics," *J. Achiev. Mater. Manuf. Eng.*, vol. 99, no. 1, pp. 14–41, 2020.

[13] L.A. Dobrzański, L.B. Dobrzański, and A.D. Dobrzańska-Danikiewicz, "Overview of conventional technologies using the powders of metals, their alloys and ceramics in Industry 4.0 stage," *J. Achiev. Mater. Manuf. Eng.*, vol. 98, no. 2, pp. 56–85, 2020.

[14] K. Cesarz-Andraczke and A. Kazek-Kęsik, "PEO layers on Mg-based metallic glass to control hydrogen evolution rate," *Bull. Polish Acad. Sci. Tech. Sci.*, vol. 68, no. 1, pp. 119–124, 2020.

[15] M.K. Datta *et al.*, "Structure and thermal stability of biodegradable Mg-Zn-Ca based amorphous alloys synthesized by mechanical alloying," *Mater. Sci. Eng. B*, vol. 176, no. 20, pp. 1637–1643, Dec. 2011.

[16] S.A. Abdel-Gawad and M.A. Shoeib, "Corrosion studies and microstructure of Mg-Zn-Ca alloys for biomedical applications," *Surf. Interfaces*, vol. 14, no. August 2018, pp. 108–116, 2019.

[17] M. Krämer *et al.*, "Corrosion behavior, biocompatibility and biomechanical stability of a prototype magnesium-based biodegradable intramedullary nailing system," *Mater. Sci. Eng. C*, vol. 59, pp. 129–135, 2016.

[18] J. Kuhlmann *et al.*, "Fast escape of hydrogen from gas cavities around corroding magnesium implants," *Acta Biomater.*, vol. 9, no. 10, pp. 8714–8721, 2013.

[19] B. Hrapkowicz and S.T. Lesz, "Characterization of Ca 50 Mg 20 Zn 12 Cu 18 Alloy," *Arch. Foundry Eng.*, vol. 19, no. 1, pp. 75–82, 2019.

[20] J. Wilson, *Metallic biomaterials*. Elsevier Ltd, 2018.

[21] H.J. Yu, J.Q. Wang, X.T. Shi, D. V. Louzguine-Luzgin, H.K. Wu, and J.H. Perepezko, "Ductile biodegradable Mg-based metallic glasses with excellent biocompatibility," *Adv. Funct. Mater.*, vol. 23, no. 38, pp. 4793–4800, 2013.

[22] B. Zberg, P.J. Uggowitzer, and J.F. Löffler, "MgZnCa glasses without clinically observable hydrogen evolution for biodegradable implants," *Nat. Mater.*, vol. 8, p. 887, Sep. 2009.

[23] J. Byrne, E. O'Cearbhaill, and D. Browne, "Comparison of crystalline and amorphous versions of a magnesium-based alloy: corrosion and cell response," *Eur. Cells Mater.*, vol. 30, no. Supplement 3, p. 75, 2015.

[24] O. Baulin, D. Fabrègue, H. Kato, A. Liens, T. Wada, and J.M. Pelletier, "A new, toxic element-free Mg-based metallic glass for biomedical applications," *J. Non. Cryst. Solids*, vol. 481, no. September 2017, pp. 397–402, 2018.

[25] M.B. Kannan and R.K.S. Raman, "In vitro degradation and mechanical integrity of calcium-containing magnesium alloys in modified-simulated body fluid," *Biomaterials*, vol. 29, no. 15, pp. 2306–2314, 2008.

[26] M. Salahshoor and Y.B. Guo, "Biodegradation control of magnesium-calcium biomaterial via adjusting surface integrity by synergistic cutting-burnishing," *Procedia CIRP*, vol. 13, pp. 143–149, 2014.

[27] H. Wang, Y. Estrin, and Z. Zúberová, "Bio-corrosion of a magnesium alloy with different processing histories," *Mater. Lett.*, vol. 62, no. 16, pp. 2476–2479, 2008.

[28] Y. Guangyin, L. Manping, D. Wenjiang, and A. Inoue, "Microstructure and mechanical properties of Mg-Zn-Si-based alloys," *Mater. Sci. Eng. A*, vol. 357, no. 1–2, pp. 314–320, 2003.

[29] Z. Liang *et al.*, "Effects of Ag, Nd, and Yb on the microstructures and mechanical properties of Mg-Zn-Ca metallic glasses," *Metals (Basel).*, vol. 8, no. 10, pp. 1–10, 2018.

[30] S. Lesz, T. Tański, B. Hrapkowicz, M. Karolus, J. Popis, and K. Wiechniak, "Characterisation of Mg-Zn-Ca-Y powders manufactured by mechanical milling," *J. Achiev. Mater. Manuf. Eng.*, vol. 103, no. 2, pp. 49–59, 2020.

[31] S.M. Al Azar and A.A. Mousa, *Mechanical and physical methods for the metal oxide powders production*. INC, 2020.

[32] I. Polmear, D. StJohn, J.-F. Nie, and M. Qian, *Novel Materials and Processing Methods*. 2017.

[33] C. Liu, Z. Ren, Y. Xu, S. Pang, X. Zhao, and Y. Zhao, "Biodegradable Magnesium Alloys Developed as Bone Repair Materials: A Review," *Scanning*, vol. 2018. 2018.

[34] M. Pogorielov, E. Husak, A. Solodivnik, and S. Zhdanov, "Magnesium-based biodegradable alloys: Degradation, application, and alloying elements," *Interventional Med. Appl. Sci.*, vol. 9, no. 1. pp. 27–38, 2017.

[35] Y.Q. Tang, Q.Y. Wang, Q.F. Ke, C.Q. Zhang, J.J. Guan, and Y.P. Guo, "Mineralization of ytterbium-doped hydroxyapatite nanorod arrays in magnetic chitosan scaffolds improves osteogenic and angiogenic abilities for bone defect healing," *Chem. Eng. J.*, vol. 387, no. January, p. 124166, 2020.

[36] C. Suryanarayana, "Mechanical alloying and milling," *Prog. Mater Sci.*, vol. 46, no. 1–2. Pergamon, pp. 1–184, 01-Jan-2001.

[37] M. Karolus, "Applications of Rietveld refinement in Fe-B-Nb alloy structure studies," *J. Mater. Process. Technol.*, vol. 175, no. 1–3, pp. 246–250, 2006.

[38] L.A. Dobrzański, B. Tomiczek, G. Matula, and K. Gołombek, "Role of Halloysite Nanoparticles and Milling Time on the Synthesis of AA 6061 Aluminium Matrix Composites," *Adv. Mater. Res.*, vol. 939, pp. 84–89, May 2014.

[39] M. Jurczyk, *Bionanomaterials for Dental Applications*. Pan Stanford Publishing, 2012.